RSC Advances

PAPER

View Article Online
View Journal | View Issue

Check for updates

Cite this: *RSC Adv.*, 2026, **16**, 12725

Hinokitiol-fueled disks form exclusionary zones in the presence of iron

Lara Rae Holstein, [ab] Megan S. Santamore,[a] Asahi Tsukamoto,[a] Masayuki Takeuchi, [ab] Nobuhiko J. Suematsu [c] and Atsuro Takai *[ab]

Stimuli-responsive, directional motions, such as chemotaxis, are vital for the development of sophisticated synthetic systems with autonomous motility. Here, we demonstrate that disks containing hinokitiol exhibit directional self-propelled motion on water in response to metal ions, particularly Fe(III) ion. The self-propelled motion arises from surface tension gradients at the air-water interface, generated by the asymmetric release of hinokitiol, which induce Marangoni flows that propel the disks. Upon contact with Fe(III), hinokitiol forms a highly surface-active complex that locally lowers the surface tension and establishes a persistent interfacial gradient. This localized accumulation of the iron complex acts as a chemo-repulsive signal, directing the disks away from iron-rich regions and leading to the formation of exclusionary zones that influence the trajectories of subsequent disks. These findings demonstrate how self-secreted chemical signals can generate interfacial memory and communication in macroscopic active systems, providing a molecular design principle for life-like collective behavior.

Received 17th February 2026
Accepted 25th February 2026

DOI: 10.1039/d6ra01403h

rsc.li/rsc-advances

Open Access Article. Published on 06 March 2026. Downloaded on 5/25/2026 4:46:43 AM.
This article is licensed under a Creative Commons Attribution-NonCommercial 3.0 Unported Licence.

Introduction

Directional locomotion in response to chemical stimuli represents an essential biological process known as chemotaxis.[1] Motion away from chemo-repellent species, termed negative chemotaxis, serves as a communication mechanism between individuals that not only enables organisms to migrate from unfavorable conditions,[2] but is also vital for the assembly of neural networks through the creation of exclusionary zones.[3] Reproduction of such chemo-repulsive behaviors in synthetic systems provides opportunities to model physical parameters of biological systems which could serve as a framework for next generation responsive materials that exhibit memory and patterned self-assembly.[4] To this end, Marangoni flow has emerged as a popular avenue by which synthetic, self-propelling objects can be achieved through interfacial surface tension gradients, which are typically generated by the release of surface-active "fuel" species.[5] Some Marangoni motors can be made to display rudimentary chemotactic behaviors for communication and maze-solving when used in conjunction with chemical reactions,[6] pre-existing gradients,[7] or solute-mediated interactions.[8] Despite these advances, examples of macroscopic-level communicative behaviors through self-secreted signals remain rare—particularly in the realm of chemo-repulsive systems.

Herein, we demonstrate that disks containing hinokitiol (**HT**) autonomously exhibit negative chemotaxis toward aqueous iron, generating exclusionary zones. Inspired not only by the biochemical[9] and self-propelling[10] properties of **HT**, but also by its ability to bind and transport a range of metal ions,[11] we envisioned that **HT** could be utilized as a potential chemotactic fuel enabling synthetic systems to respond to metal ions. Furthermore, building on our previous reports that disks composed of fuel and a polymer scaffold can undergo consistent and tunable self-propelled motion on aqueous surfaces, we employed polystyrene-polyisoprene elastomer (**SIS**) as a scaffold to construct symmetrical disks, thereby eliminating shape-dependent effects on motion.[10,12] While examples of changes in autonomous behaviors induced by metal ion complexation have been reported,[13] this system represents a unique example of a macroscopic object displaying negative chemotaxis by producing a chemo-repellent that is more surface-active than its own fuel (Fig. 1a).

Results and discussion

The complexation of **HT** with ferric ions (Fe^{3+}) has been reported to proceed in a 3 : 1 molar ratio in buffer solution (pH 7.0).[11b] To confirm this coordination behavior under our conditions, we carried out titration experiments using UV-vis absorption spectroscopy. An aqueous solution of **HT** (30 μM) at pH 7 was titrated with $FeCl_3 \cdot 6H_2O$ at 25 °C. As shown in

[a]*Molecular Design and Function Group, National Institute for Materials Science (NIMS), 1-2-1 Sengen, Tsukuba, Ibaraki 305-0047, Japan. E-mail: TAKAI.Atsuro@nims.go.jp*

[b]*Department of Materials Science and Engineering, Faculty of Pure and Applied Sciences, University of Tsukuba, 1-1-1 Tennodai, Tsukuba, Ibaraki 305-8577, Japan*

[c]*School of Interdisciplinary Mathematical Sciences, Graduate School of Advanced Mathematical Sciences, Meiji Institute for Advanced Study of Mathematical Sciences (MIMS), Meiji University, 4-21-1, Nakano, Tokyo 164-8525, Japan*

© 2026 The Author(s). Published by the Royal Society of Chemistry

Open Access Article. Published on 06 March 2026. Downloaded on 5/25/2026 4:46:43 AM.
This article is licensed under a Creative Commons Attribution-NonCommercial 3.0 Unported Licence.

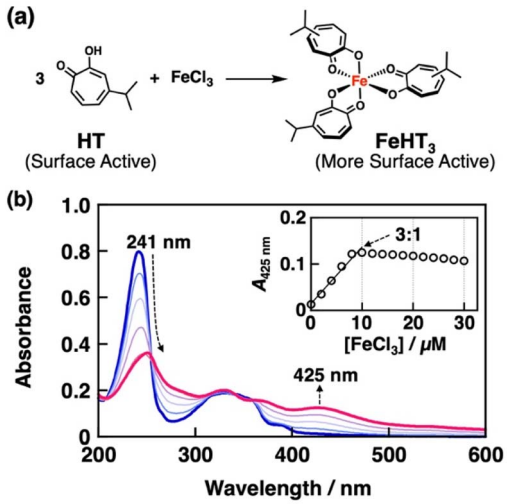

Fig. 1 (a) Reaction between HT and aqueous $FeCl_3$ to yield the surface-active complex, $FeHT_3$. (b) UV-vis absorption spectral changes of HT (30 μM, blue) upon addition of $FeCl_3$ to form a 3 : 1 complex (pink) in distilled water at 25 °C. Inset shows the plot of the absorbance at 425 nm *vs.* [$FeCl_3$].

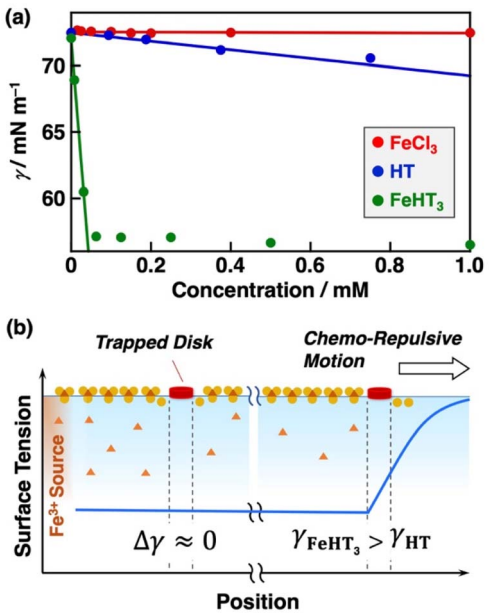

Fig. 2 (a) Concentration-dependent surface tension of $FeCl_3$ (red), HT (blue), and $FeHT_3$ complex (green) in distilled water at 25 °C. (b) Schematic illustration of the self-confinement and chemo-repulsion mechanisms due to the surface accumulation of $FeHT_3$.

Fig. 1b, the absorption band of **HT** at 241 nm gradually decreased and red-shifted, accompanied by the emergence of a new absorption band at 425 nm. The intensity of the 425 nm band reached saturation upon the addition of 10 μM Fe^{3+}. These results indicate that **HT** and Fe^{3+} form a 3 : 1 complex (**$FeHT_3$**). The absorbance at 425 nm slightly decreased at concentrations of $FeCl_3$ above 10 μM, probably due to partial precipitation of **$FeHT_3$** during the UV-vis absorption titration measurements (over 30 min). Such precipitation behavior may also obscure a precise Job plot analysis for confirming the stoichiometry under the present conditions. Nevertheless, 3 : 1 complex formation was further supported by mass spectrometric analysis (see Fig. S1) as well as previously reported single-crystal X-ray structural analyses obtained under analogous conditions.[11b] Given that complex formation was essentially quantitative even near the lowest concentrations accessible by UV-vis absorption titration, the stability constant of **$FeHT_3$** is estimated to be greater than 10^{18} M^{-3}.

Also, **HT** is known to form metal complexes with various stoichiometries, including 1 : 2 complexes with divalent metal ions.[11b,14] First, to examine whether the identity of the counter-anion affects the complexation behavior of **HT** with Fe^{3+}, UV-vis absorption titration was performed using $Fe(NO_3)_3 \cdot 9H_2O$ under conditions analogous to those used for $FeCl_3$ (Fig. S2a). Although the concentration of $Fe(NO_3)_3$ required to reach saturation was slightly higher than that of $FeCl_3$, the final absorption spectrum obtained after saturation was essentially identical to that observed in the presence of $FeCl_3$, indicating the formation of the same **$FeHT_3$** complex. Next, we examined the complexation behavior of **HT** with $FeCl_2 \cdot 4H_2O$ and $CuCl_2 \cdot 2H_2O$ under conditions analogous to those used for $FeCl_3$. In both cases, complex formation was observed (see Fig. S2b and S2c). Although a direct quantitative comparison is not straightforward due to differences in coordination modes between trivalent and divalent metal complexes, the **$FeHT_3$** complex formation is particularly stable and exhibited a simple and well-defined change in the UV-vis absorption spectrum.

To investigate the effect of **$FeHT_3$** formation on the self-propelled motion of **HT** at the air-water interface, the swimming behavior of pristine **HT** clumps and **HT-SIS** disks was monitored in a circular Petri dish on a homogeneous solution of aqueous $FeCl_3$ at different concentrations (see SI for the experimental setup). Overall, pristine **HT** clumps displayed rapid continuous motions on aqueous $FeCl_3$ solution (Fig. S3; SI Movie 1). **HT-SIS** disks exhibited similar self-propelled behavior before coming to a halt as they became confined by an increasingly shrinking barrier in the presence of $FeCl_3$ (SI Movie 2). Notably, the distinct switching behavior from continuous to oscillatory motion observed in the absence of $FeCl_3$ became much less apparent.[10] Compared to pristine **HT** clumps, **HT-SIS** disks, which represent a lower supply of **HT**, continued to swim longer than pristine **HT** clumps. The motion was maintained the longest at low iron concentrations (10 μM, Fig. S4a). As the concentration of $FeCl_3$ was increased to 50 μM, the duration of the self-propelled motion decreased (Fig. S4b): a trend that continued at high iron concentrations (100 μM, Fig. S4c). After coming to a halt on a 100 μM $FeCl_3$ solution, a **HT-SIS** disk transferred to fresh iron solution resumed motion while a second **HT-SIS** disk placed on the original solution did not move (Fig. S5). These observations indicate that the accumulation of **$FeHT_3$** on the surface can hinder self-propelled motion by trapping the disk.

To assess the possible influence of counter-anions on motion behavior, self-propelled motion of **HT-SIS** disks was studied using $Fe(NO_3)_3$ instead of $FeCl_3$. The resulting self-

© 2026 The Author(s). Published by the Royal Society of Chemistry

Open Access Article. Published on 06 March 2026. Downloaded on 5/25/2026 4:46:43 AM.
This article is licensed under a Creative Commons Attribution-NonCommercial 3.0 Unported Licence.

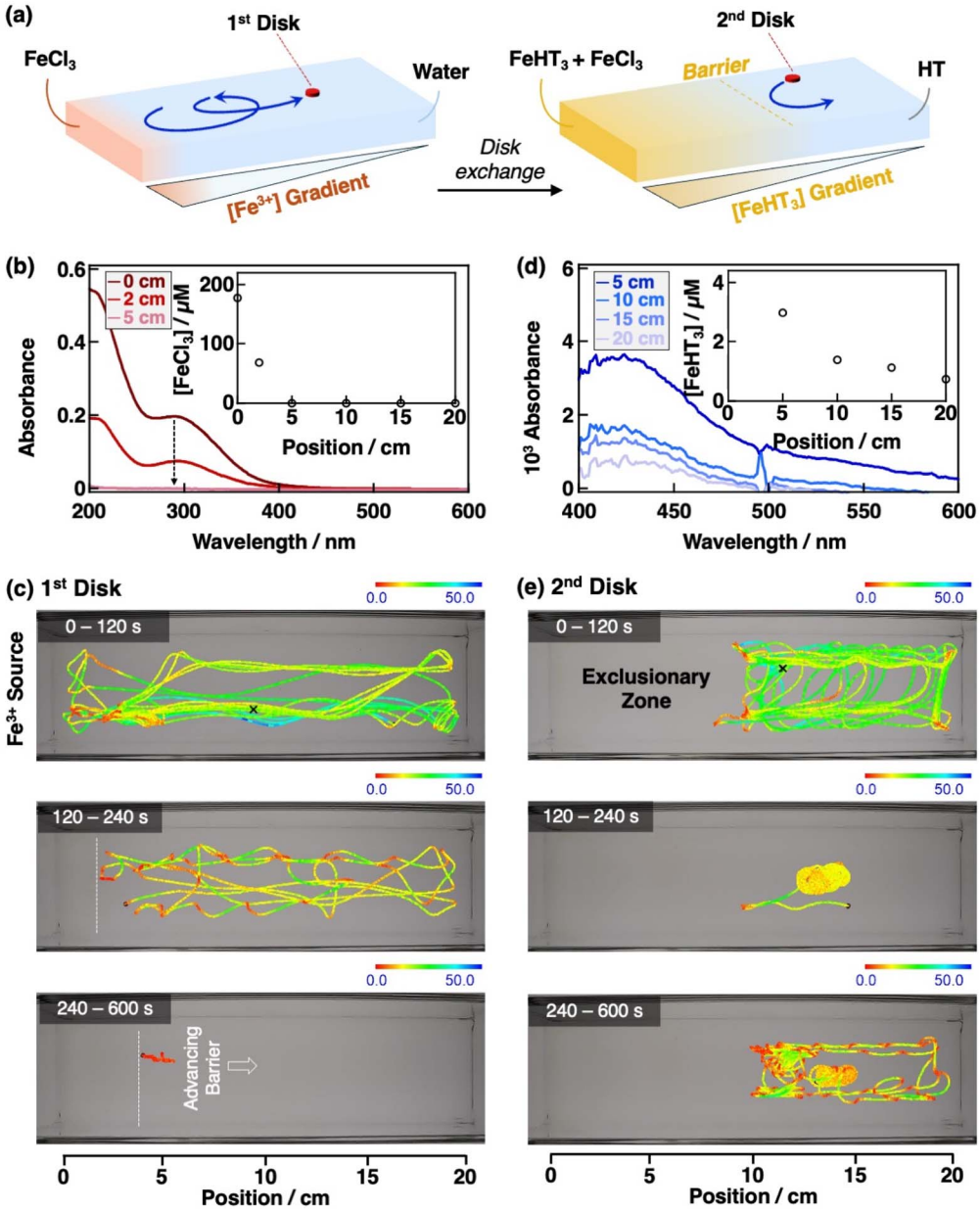

Fig. 3 (a) Schematic illustration of the aqueous conditions during the chemotactic motions of the first and second **HT-SIS** disks. (b) UV-vis absorption spectra recorded at different positions from the Fe^{3+} source, measured 5 min after placing aqueous $FeCl_3$ at the 0 cm position. The inset shows the calculated $FeCl_3$ concentrations based on the absorption coefficient at 300 nm (1.07×10^4 M^{-1} cm^{-1}). (c) Trajectories of the first **HT-SIS** disk on an Fe^{3+} gradient. (d) UV-vis absorption spectra showing the band assigned to $\mathbf{FeHT_3}$ at different positions after the first disk had been allowed to swim for 600 s. The inset shows the calculated $\mathbf{FeHT_3}$ concentrations based on the absorption coefficient at 425 nm (1.20×10^4 M^{-1} cm^{-1}). (e) Trajectories of a second **HT-SIS** disk in the presence of the $\mathbf{FeHT_3}$ barrier generated by the first disk. In (c) and (e), the color bar represents the average speed (mm s^{-1}) of the disk. The approximate starting points of the first and second disks are indicated with an *x*.

propelled behaviors were comparable to those observed for $FeCl_3$ (Fig. S6a), indicating that the observed chemotactic response is largely insensitive to the nature of the counter-anion under the present conditions. Similarly, self-propelled motion was observed using $FeCl_2$ and $CuCl_2$ as alternative metal ion sources. The behavior of disks in the presence of $FeCl_2$ showed no obvious deviation from that observed for $FeCl_3$ (Fig. S6b). By contrast, although **HT** is expected to form a complex with Cu^{2+} that may influence the interfacial properties, no self-trapping of the disk was observed (Fig. S6c). These results highlight the importance of the strong and surface-localized formation of an iron-**HT** complex, especially $\mathbf{FeHT_3}$, in generating sustained chemotactic confinement.

To understand the mechanism underlying the change in self-propelled behavior upon $\mathbf{FeHT_3}$ formation, concentration-dependent surface tension (γ) measurements were conducted using the Wilhelmy plate method (Fig. 2a). As the concentration increased, the surface tension of $\mathbf{FeHT_3}$ solutions dropped

Open Access Article. Published on 06 March 2026. Downloaded on 5/25/2026 4:46:43 AM. This article is licensed under a Creative Commons Attribution-NonCommercial 3.0 Unported Licence.

much more steeply than that of **HT** solutions, eventually reaching 57 mN m^{-1}. This value is lower than the saturated surface tension observed for **HT** aqueous solutions, which plateaued at 62 mN m^{-1} above 2.5 mM.[10] A linear approximation in the low-concentration region ($\gamma = \gamma_0 - a[C]$, where γ_0 is the surface tension of distilled water, 72 mN m^{-1}, and C is the solute concentration) yielded an a value of 368 N m^{-1} M^{-1} for **$FeHT_3$**, in contrast to 4.8 N m^{-1} M^{-1} for **HT**, indicating a markedly higher surface activity of the **$FeHT_3$** complex. Meanwhile, the surface tension of $FeCl_3$ aqueous solutions remained nearly unchanged under the conditions used in this study. These results indicate that both **HT** and **$FeHT_3$** act as surface-active species responsible for the observed self-propelled motion *via* Marangoni flow. Importantly, although **$FeHT_3$** exhibits higher surface activity than **HT**, its primary role is not to enhance propulsion but to define the directionality of motion. While **HT** is released continuously from the disk and generates transient surface tension gradients that sustain motion, **$FeHT_3$** is produced locally upon contact between **HT** and Fe^{3+} and remains strongly adsorbed at the air-water interface, generating persistent, localized reductions in surface tension (Fig. 2b). This leads to the formation of a relatively persistent, spatially localized low surface tension region. Consequently, the disk is subjected to a sustained Marangoni force directed toward regions of higher surface tension, leading to consistent repulsion from iron-rich areas rather than altered propulsion dynamics.

Because the high surface activity of **$FeHT_3$** enables it to function as a chemo-repulsive signal, we examined the chemotactic behavior of **HT-SIS** disks in an environment where iron is not homogenously available (Fig. 3a). A 20 μL droplet of aqueous $FeCl_3$ was placed along the left edge (0 cm position) of a rectangular container (5 × 20 cm) filled with water to a depth of 3 mm. The first **HT-SIS** disk was placed in the center of the dish (10 cm from the left edge) 5 min later. UV-vis spectroscopy indicated a sharp Fe^{3+} concentration gradient localized near the 0 cm position (Fig. 3b). The first disk exhibited stochastic, negative chemotaxis away from the iron source (Fig. 3c). In the first 120 s the disk moved ballistically across the entire dish, briefly slowing as it passed through the iron-rich region (SI Movie 3). Within the next 120 s, the disk appeared to become trapped for several seconds near the 2 cm position before bursting free and transitioning to oscillatory motion, now avoiding the furthermost left side of the dish (SI Movie 4). Finally, after becoming trapped at 4 cm, the disk cycled between periods where it began to shake in place, becoming increasingly more violent before moving slightly toward the 20 cm position (SI Movie 5).

After 600 s, the first disk was removed, and a second disk was placed in the center of the dish. UV-vis absorption spectral analysis of the aqueous phase at different positions following the motion of the first **HT-SIS** disk for 600 s confirmed the formation of an **$FeHT_3$** concentration gradient (Fig. 3d). The second disk appeared to rebound from an invisible barrier (Fig. 3e, SI Movie 6), indicating that an exclusionary zone had been established by the chemo-repulsive **$FeHT_3$** generated through the first disk's contact with iron.

The trajectories of both the first and second **HT-SIS** disks tended to shift to the right over time, suggesting diffusion of **$FeHT_3$**. As a result, the system developed a persistent surface tension gradient, which also enabled a disk composed solely of **SIS** to migrate toward the right when placed on the surface after 600 s (Fig. S7). Similarly, when a third **HT-SIS** disk was introduced within the exclusionary zone, it was directed away from the iron source; meanwhile, the second disk remained outside (Fig. S8). These results demonstrate that environmental modification by the first disk can direct both fueled and fuel-free objects through interfacial gradient formation.

Notably, the size of the exclusionary zone appeared to depend strongly on the behavior of the first disk. Brief iron exposure resulted in the formation of **$FeHT_3$** on the disk surface which could provide a strong driving force for ballistic motion across the dish. Repeated returns to the iron-rich region of the gradient ensured the continued production of **$FeHT_3$** which could eventually trap the **HT**-secreting disk near the iron source as exhibited in Fig. 3c, when the first disk remained near the 5 cm position for *ca.* 380 s. As a result, complexation could occur continuously, causing the surface pressure to increase and the exclusionary zone to expand to the 10 cm position. Conversely, in the case of the second **HT-SIS** disk in Fig. 3e, the barrier did not shift significantly because **HT** was not released in an iron-rich environment. On the other hand, when the first disk was trapped for *ca.* 190 s at 5.5 cm, the exclusionary zone did not expand beyond the 6 cm position (Fig. S9). Thus, the environment is characteristically modified by the behavior of the first disk, allowing it to direct itself and others away from the iron source. This behavior demonstrates that **HT-SIS** disks can exhibit rudimentary memory effects and indirect, environment-mediated interactions with other Marangoni motors in a manner that is conceptually analogous to living systems.

Conclusions

In conclusion, we have demonstrated that self-propelled, **HT**-fueled disks on the surface of water can respond to aqueous iron through the formation of the surface-active complex **$FeHT_3$**. The interplay between **HT** release, **$FeHT_3$** formation, and their distinct surface activities governs the emergence of negative chemotaxis, enabling the disks to direct their self-propelled motion *via* Marangoni flows. Importantly, the locally produced **$FeHT_3$** functions as a chemo-repulsive signal that not only directs and confines the motion of the disk but also influences subsequent disks through the generation of exclusionary zones. These findings reveal how self-secreted chemical species can mediate communication and environmental memory in self-propelled systems. The present study thus provides a molecular design framework for the development of advanced responsive materials capable of adaptive, life-like motion.

Author contributions

Lara Rae Holstein: conceptualization, investigation, writing – original draft, writing – review & editing. Megan S. Santamore: investigation. Asahi Tsukamoto: investigation. Masayuki

© 2026 The Author(s). Published by the Royal Society of Chemistry

Open Access Article. Published on 06 March 2026. Downloaded on 5/25/2026 4:46:43 AM. This article is licensed under a Creative Commons Attribution-NonCommercial 3.0 Unported Licence.

Takeuchi: writing – review & editing. Nobuhiko J. Suematsu: software, writing – review & editing. Atsuro Takai: conceptualization, supervision, funding acquisition, writing – original draft, writing – review & editing.

Conflicts of interest

There are no conflicts to declare.

Data availability

The data supporting this article have been included as part of the supplementary information (SI). Supplementary information is available. See DOI: https://doi.org/10.1039/d6ra01403h.

Acknowledgements

We are grateful to Ms. Izumi Matsunaga (NIMS) for her assistance with the experiments. This work was supported by a Grant-in-Aid for Scientific Research on KAKENHI (Grant Numbers: JP21H01004, JP23K03347, JP24K01475, and JP23K04725), a Grant-in-Aid for Transformative Research Areas (A) "Materials Science of Meso-Hierarchy" (Grant Number: JP24H01734), and the Inamori Foundation. We also thank support from ARIM of MEXT (JPMXP1224NM5109 and JPMXP1225NM5064) and MEXT's Promotion of Distinctive Joint Usage/Research Center Support Program (JPMXP0724020292).

References

1 (*a*) J. Adler, *Science*, 1966, **153**, 708; (*b*) V. Kundra, J. A. Escobedo, A. Kazlauskas, H. K. Kim, S. G. Rhee, L. T. Williams and B. R. Zetter, *Nature*, 1994, **367**, 474; (*c*) G. H. Wadhams and J. P. Armitage, *Nat. Rev. Mol. Cell Biol.*, 2004, **5**, 1024.

2 (*a*) M. Zaki, N. Andrew and R. H. Insall, *Proc. Natl. Acad. Sci. U. S. A.*, 2006, **103**, 18751; (*b*) J. E. Phillips and R. H. Gomer, *Proc. Natl. Acad. Sci. U. S. A.*, 2012, **109**, 10990.

3 (*a*) A. Pini, *Science*, 1993, **261**, 95; (*b*) O. Marín, A. Yaron, A. Bagri, M. Tessier-Lavigne and J. L. R. Rubenstein, *Science*, 2001, **293**, 872.

4 (*a*) B. Liebchen, D. Marenduzzo, I. Pagonabarraga and M. E. Cates, *Phys. Rev. Lett.*, 2015, **115**, 258301; (*b*) K. Feng, J. C. Ureña Marcos, A. K. Mukhopadhyay, R. Niu, Q. Zhao, J. Qu and B. Liebchen, *Adv. Sci.*, 2023, **10**, 2300866; (*c*) T. Sugawara, M. Matsuo and T. Toyota, *Bull. Chem. Soc. Jpn.*, 2024, **98**, uoae134; (*d*) J. Kim, P. Mayorga-Burrezo, S.-J. Song, C. C. Mayorga-Martinez, M. Medina-Sánchez, S. Pané and M. Pumera, *Chem. Soc. Rev.*, 2024, **53**, 9190; (*e*) S. Krishna Mani, L. Lazinski, S. G. Birrer, A. Sapre, L. D. Zarzar and A. Sen, *J. Am. Chem. Soc.*, 2025, **147**, 47942; (*f*) C. Wu, Y. Huang, B. Zeng, J. Chen, C. H. Chu, M. Yang, H. C. Shum and J. Tang, *J. Am. Chem. Soc.*, 2025, **147**, 40225.

5 (*a*) C. Tomlinson, *Proc. R. Soc. London*, 1862, **11**, 575; (*b*) L. E. Scriven and C. V. Sternling, *Nature*, 1960, **187**, 186; (*c*) N. J. Suematsu and S. Nakata, *Chem.–Eur. J.*, 2018, **24**, 6308; (*d*) H. Yu, Y. Wang, Z. Hou, X. Xia, H. Chen, B. Zou and Y. Zhang, *Adv. Funct. Mater.*, 2025, **35**, 2424235.

6 (*a*) O. Kuksenok, P. Dayal, A. Bhattacharya, V. V. Yashin, D. Deb, I. C. Chen, K. J. Van Vliet and A. C. Balazs, *Chem. Soc. Rev.*, 2013, **42**, 7257; (*b*) Y. Yasugahira, Y. Tatsumi, O. Yamanaka, H. Nishimori, M. Nagayama and S. Nakata, *ChemSystemsChem*, 2022, **4**, e202100031; (*c*) D. Babu, N. Katsonis, F. Lancia, R. Plamont and A. Ryabchun, *Nat. Rev. Chem.*, 2022, **6**, 377; (*d*) Y. Hamano, K. Ikeda, K. Odagiri and N. J. Suematsu, *Sci. Rep.*, 2023, **13**, 8173; (*e*) M. Matsuo, K. Ejima and S. Nakata, *J. Colloid Interface Sci.*, 2023, **639**, 324; (*f*) M. Dindo, A. Bevilacqua, G. Soligo, V. Calabrese, A. Monti, A. Q. Shen, M. E. Rosti and P. Laurino, *J. Am. Chem. Soc.*, 2024, **146**, 15965.

7 (*a*) I. Lagzi, S. Soh, P. J. Wesson, K. P. Browne and B. A. Grzybowski, *J. Am. Chem. Soc.*, 2010, **132**, 1198; (*b*) C. Jin, C. Krüger and C. C. Maass, *Proc. Natl. Acad. Sci. U. S. A.*, 2017, **114**, 5089; (*c*) T. Furuki, H. Sakuta, N. Yanagisawa, S. Tabuchi, A. Kamo, D. S. Shimamoto and M. Yanagisawa, *ACS Appl. Mater. Interfaces*, 2024, **16**, 43016.

8 (*a*) C. H. Meredith, P. G. Moerman, J. Groenewold, Y.-J. Chiu, W. K. Kegel, A. van Blaaderen and L. D. Zarzar, *Nat. Chem.*, 2020, **12**, 1136; (*b*) A. van der Weijden, M. Winkens, S. M. C. Schoenmakers, W. T. S. Huck and P. A. Korevaar, *Nat. Commun.*, 2020, **11**, 4800.

9 (*a*) T. Nozoe, *Bull. Chem. Soc. Jpn.*, 1936, **11**, 295; (*b*) H. Erdtman and J. Gripenberg, *Nature*, 1948, **161**, 719; (*c*) Z. Jian and Z. Jian, *Curr. Med. Chem.*, 2007, **14**, 2597; (*d*) G. Sennari, R. Saito, T. Hirose, M. Iwatsuki, A. Ishiyama, R. Hokari, K. Otoguro, S. Ōmura and T. Sunazuka, *Sci. Rep.*, 2017, **7**, 7259; (*e*) M. S. Bhuia, R. Chowdhury, M. Afroz, M. S. Akbor, M. S. Al Hasan, J. Ferdous, R. Hasan, M. V. O. B. de Alencar, M. S. Mubarak and M. T. Islam, *Chem. Biodiversity*, 2025, **22**, e202401904.

10 L. R. Holstein, M. Takeuchi, N. J. Suematsu and A. Takai, *J. Am. Chem. Soc.*, 2025, **147**, 40024.

11 (*a*) P. L. Pauson, *Chem. Rev.*, 1955, **55**, 9; (*b*) A. S. Grillo, A. M. SantaMaria, M. D. Kafina, A. G. Cioffi, N. C. Huston, M. Han, Y. A. Seo, Y. Y. Yien, C. Nardone, A. V. Menon, J. Fan, D. C. Svoboda, J. B. Anderson, J. D. Hong, B. G. Nicolau, K. Subedi, A. A. Gewirth, M. Wessling-Resnick, J. Kim, B. H. Paw and M. D. Burke, *Science*, 2017, **356**, 608.

12 L. R. Holstein, N. J. Suematsu, M. Takeuchi, K. Harano, T. Banno and A. Takai, *Angew. Chem., Int. Ed.*, 2024, **63**, e202410671.

13 (*a*) S. Nakata, S.-i. Hiromatsu and H. Kitahata, *J. Phys. Chem. B*, 2003, **107**, 10557; (*b*) K. Iida, N. J. Suematsu, Y. Miyahara, H. Kitahata, M. Nagayama and S. Nakata, *Phys. Chem. Chem. Phys.*, 2010, **12**, 1557.

14 (*a*) M. C. Barret, M. F. Mahon, K. C. Molloy, J. W. Steed and P. Wright, *Inorg. Chem.*, 2001, **40**, 4384; (*b*) Q. Gaydon and D. S. Bohle, *Inorg. Chem.*, 2021, **60**, 13567.

© 2026 The Author(s). Published by the Royal Society of Chemistry